Electrostatic Frequency Tuning of a Quatrefoil Suspension Gyroscope

Madan Parajuli, Guillermo Sobreviela, Ashwin A. Seshia
Nanoscience Centre, Department of Engineering, University of Cambridge
Cambridge, UK

***Abstract*—MEMS gyroscopes based on axisymmetric structures rely on the Coriolis coupling between near-degenerate vibration modes as the basis for the measurement of rotation rate. Significant gains in mechanical sensitivity are achieved when the natural frequencies of the two modes are perfectly matched. This paper outlines a systematic approach to mode-matching for a vacuum packaged MEMS gyroscope with a novel quatrefoil suspension system fabricated on a (100) single-crystal silicon (SCS) substrate. This approach identifies mode orientation, implements mode-to-electrode alignment, and electrostatically varies the effective stiffness of one mode to achieve a mode-matched condition. Axisymmetric ring and disc gyroscopes fabricated on a (100) SCS substrate exhibit degeneracy of the higher-order elliptical modes. However, fabrication imperfections and anchoring arrangements can result in a non-zero frequency split between these modes which can be reduced by electrostatic frequency tuning. Frequency tuning is demonstrated in a prototype MEMS gyroscope where the frequency split between the vibration modes is reduced from 5 Hz to less than 0.01 Hz.**

***Keywords*—MEMS, Frequency, Tuning, Gyroscope, Quatrefoil Suspension Gyroscope (QSG)**

I. Introduction

A significant challenge in the design of high-performance Coriolis vibratory MEMS gyroscopes is addressing low-noise and high stability measurements of rotation about a sensitive axis. A possible approach to address this challenge is to operate the gyroscope in a mode-matched condition. This requires a precise matching of the natural frequencies of the drive and sense modes. A mode-matched operation maximizes the mechanical sensitivity for amplitude modulated (AM) and frequency modulated (FM) gyroscopes [1], [2]. This advantage has motivated the use of axisymmetric structures such as rings, discs and hemispherical objects as the preferred design for high-performance MEMS gyroscopes as they inherently display degenerate modes [3]. However, practical devices can demonstrate a non-zero frequency split between modes of interest due to material anisotropy, manufacturing imperfections and anchoring arrangements.

The frequency split between the drive and sense modes' resonance frequencies can be compensated by using either electrostatic frequency tuning [1], [4] or mass perturbation methods such as mass loading [5] and laser ablation [6]. The mass perturbation methods are challenging to implement in devices that are already vacuum encapsulated. On the other hand, mode matching by electrostatic frequency tuning method can be readily implemented in low frequency flexural gyroscopes. However, for high frequency mechanical gyroscopes it can be difficult to compensate even small mismatches in the natural frequencies due to the high mechanical stiffnesses of these modes. The mode matching using electrostatic frequency tuning in high frequency modes relies on a thorough understanding of mode alignment, appropriate approach to perfectly align the modes with the electrodes used to drive, sense and tune, and an effective strategy to define the magnitude of the tuning voltage and choice of electrode(s).

This work builds on an electrostatic frequency tuning method to implement mode-matched operation reported in [4] on a prototype device where the number of electrodes have been increased from 12 to 24. The increment in the number of electrodes allows for the implementation of mode alignment, decreasing the cross-coupling between the two modes, and allowing for a perfect match of the two modes. The novelty of the method described here lies in the use of a two-step approach adding a mode alignment phase before performing the actual tuning of the modes. This additional alignment phase, differentiating this approach from [4], significantly improves the accuracy of mode-matching, enabling a match of resonance frequencies of the drive and sense modes.

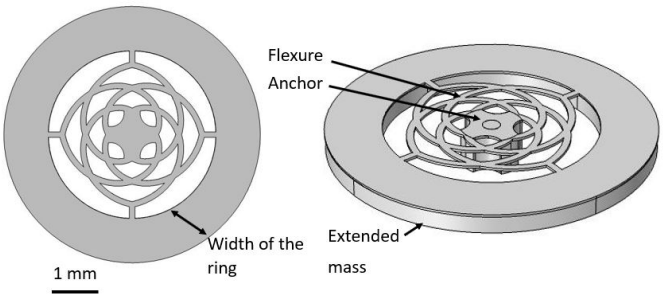

Fig. 1: Top view and perspective view of the device.

II. Device

The device-under-test in this study is a vacuum packaged micromachined disk gyroscope fabricated in a (100) single crystal silicon (SCS) substrate using a silicon-on-insulator (SOI) MEMS process employing wafer-level vacuum encapsulation [7]. The top view and perspective view of the device are shown in Fig. 1. The width of the ring is 950

μm and the inner radius of the ring is 1800 μm. The key mechanical features of this device comprise a ring supported by a quatrefoil suspension system on the central anchor [8]. The quatrefoil suspension system consists of spiral flexures winding outward from the central anchor to the ring in both clockwise and anti-clockwise directions. These design features minimize thermoelastic damping and anchor loss leading to a quality factor of over a million for the secondary elliptical modes. The ring and central anchored regions are comprised of a thicker structural layer (340 μm) while the thickness of the electrodes and flexures is 40 µm. The substantially thicker outer ring increases the effective mass of the device, and the thermomechanical noise contributions to the measurement is therefore very low. The external part of the ring is surrounded by 24 identical electrodes separated by a capacitive gap of 2 μm. The inner part of the ring is surrounded by 12 electrodes.

III. Methods

The secondary elliptical modes illustrated in Fig. 2 (rendering generated by the finite element analysis program COMSOL) are studied here to illustrate the electrostatic frequency tuning approach. Fig. 2 shows a representative electrode layout: the electrode marked in dark blue is used to drive the resonator; electrodes marked in light blue and orange are used to read the first and second modes respectively; electrodes marked in green and red are connected to tuning voltage sources A (V_a) and B (V_b) respectively. The ring is connected to the bias voltage through one of the outer electrodes, and the remaining electrodes are grounded.

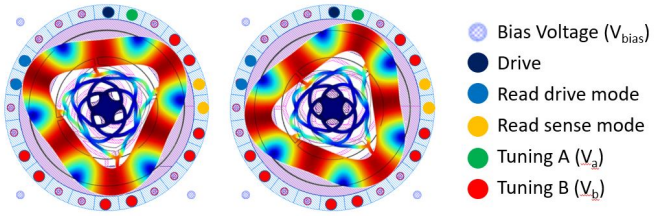

Fig. 2: The secondary degenerate modes of the device illustrated via finite element simulation (COMSOL) with the electrode configuration used for mode alignment and frequency tuning also shown.

The tuning experiment is done in two steps. In the first step, the drive and sense modes are aligned to the electrodes used for driving, sensing, and tuning by applying a voltage V_a. In the second step of the tuning experiment, V_b is applied in addition to V_a to increase the effective stiffness of the first mode. The increment of effective stiffness of the first mode increases its resonance frequency to match with the resonance frequency of the second mode.

The resonance frequency of a given mode is dependent on its mechanical stiffness k_m, electrical stiffness k_e and effective mass m (1).

$$f = \frac{1}{2\pi}\sqrt{\frac{k_m - k_e}{m}} \tag{1}$$

The mechanical stiffness and effective mass are invariant for a given mode but the electrical stiffness can be changed by changing the corresponding dc tuning voltage. As shown in the Fig. 2, the antinodes of the first mode correspond to the nodes of the second mode. However, antinodes and nodes of the modes may not be perfectly aligned with the electrodes used to drive, sense and tune the modes. Therefore, the first step is to implement mode alignment so that the dc tuning voltage (V_b) is applied on electrodes that are perfectly aligned with the antinodes of the first mode and the nodes of the second mode. The application of positive dc tuning voltage on these electrodes reduces the potential difference between the ring and the electrodes resulting in the decrement of electrical stiffness of the first mode (2) and thereby increasing the effective stiffness of the first mode without affecting the second mode.

$$k_e = \frac{\epsilon_0 \epsilon_r A (V_{bias} - V_{tuning})^2}{d^3} \tag{2}$$

where, ϵ_0 is the permittivity in vacuum, ϵ_r is the relative permittivity, A is the area of the electrode and d is the gap between the electrode and the resonator. Increased effective stiffness increases the resonance frequency of the first mode and with the application of a suitable tuning voltage, the resonance frequencies for both modes can be matched.

IV. Results

Fig. 3 and 4 plot the amplitude and phase responses sensed from the electrodes aligned with the first mode and second mode respectively for different values of V_a while driving an electrode aligned with the first mode. The decrement in amplitude and phase change with increased V_a in the zoomed regions of Fig. 3a and 3b suggest that the second mode is less aligned with the electrodes used to read the first mode. Similarly, Fig. 4a and 4b suggest that the first mode is less aligned with the electrodes used to read the second mode. These observations suggest that when V_a is 15 V, the first and second modes are perfectly aligned with the electrodes used to sense the first and the second mode respectively.

Fig. 5 and 6 plot the amplitude and phase response for drive and sense mode for different values of V_b. When V_b is increased, the resonance frequency of the first mode increases, ultimately matching with the resonance frequency of the second mode at V_a = 15 V and V_b = 29 V, decreasing the initial frequency split between the modes from 4.8 Hz to less than 0.1 Hz. This approach is successfully applied to four devices resulting in a decrease in the initial frequency split of 3.7 Hz, 4.64 Hz, 4.8 Hz and 5.06 Hz to less than 0.1 Hz in each case. The plot of the initial frequency split and required tuning voltage for mode matching for each of these four prototype devices is presented in Fig. 7.

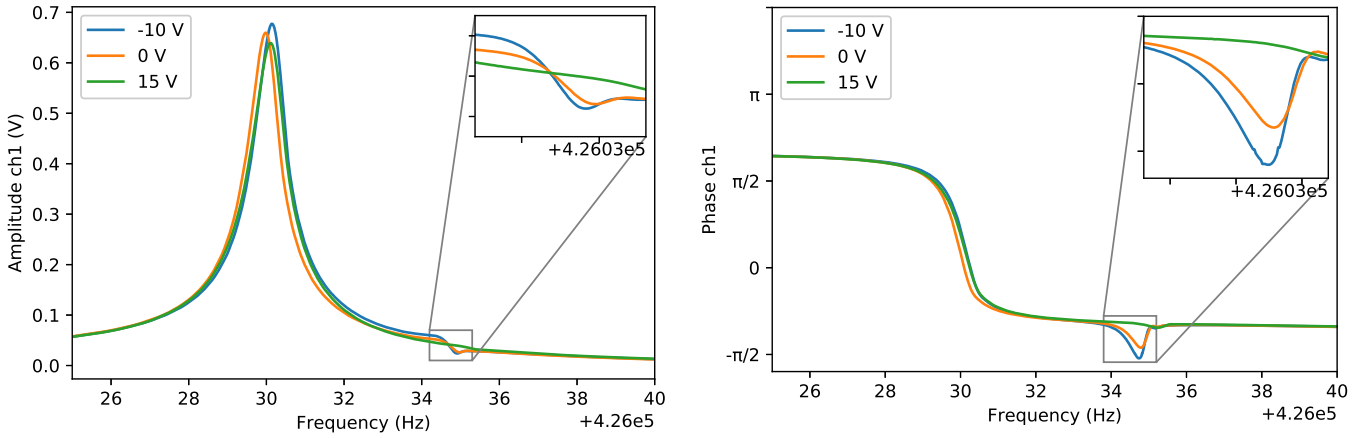

(a) (b)

Fig. 3: Amplitude and phase response sensed from the electrodes aligned with the first mode for different tuning voltages (V_as).

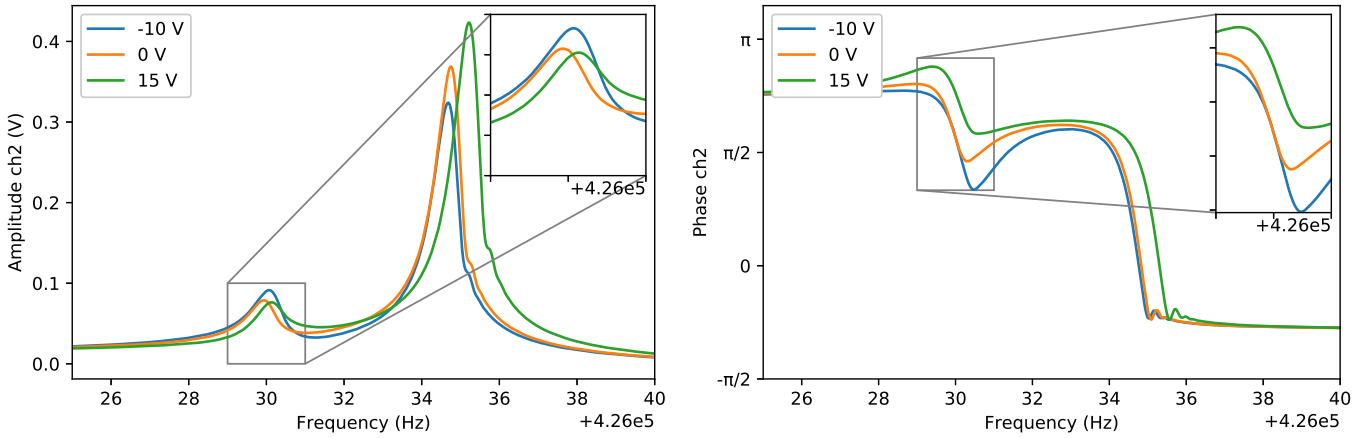

(a) (b)

Fig. 4: Amplitude and phase response sensed from the electrodes aligned with the second mode for different tuning voltages (V_as).

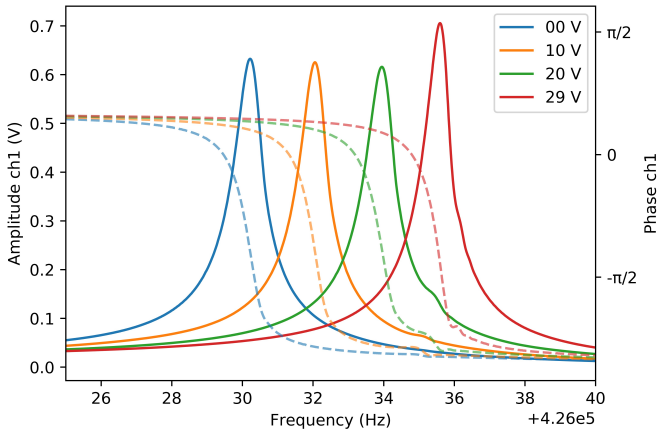

Fig. 5: Amplitude and phase responses of the first mode (drive mode) for different tuning B voltages (V_bs).

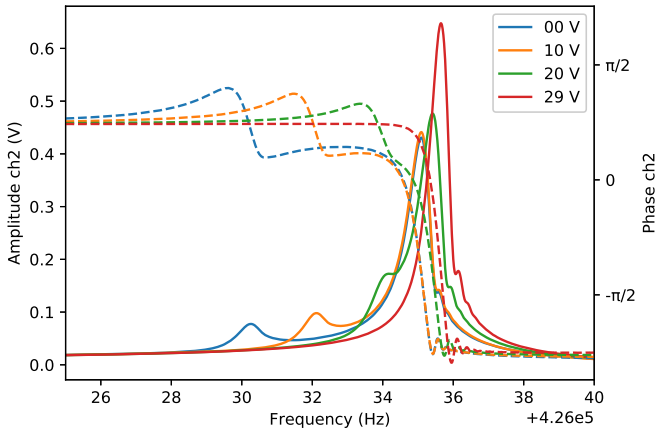

Fig. 6: Amplitude and phase responses of the second mode (sense mode) for different tuning B voltages (V_bs).

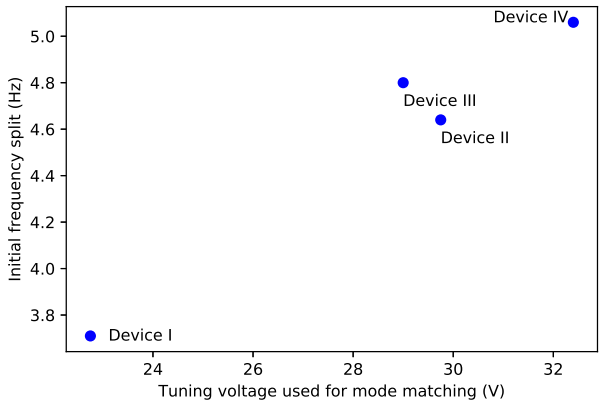

Fig. 7: Tuning voltage required to mode-match the initial frequency split of 4 different prototype devices

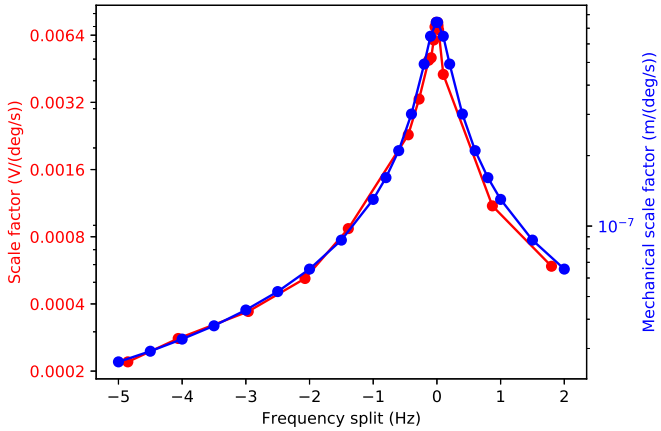

Fig. 8: Scale factor improvement for various frequency splits between the two modes.

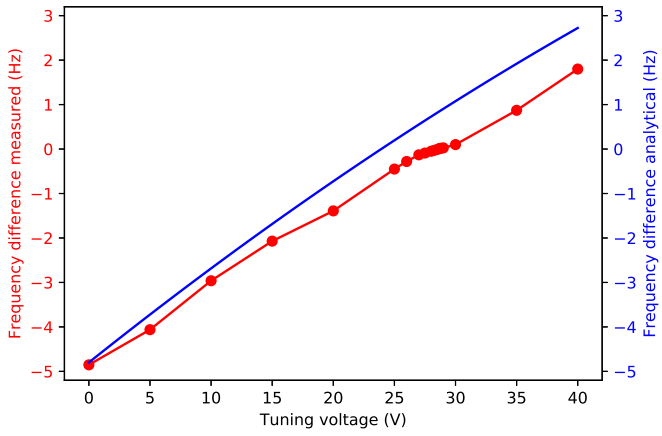

Fig. 9: Frequency split for different tuning voltages (V_b).

Fig. 8 demonstrates the measured scale factor improvement and corresponding mechanical scale factor estimation for varying degrees of mode-matching. Fig. 9 plots the frequency split as a function of tuning voltage (V_b). The analytically determined frequency difference for increased tuning voltage matches closely with the measured results as shown in Fig. 9.

V. Summary

This paper presents a two step approach to implement mode matching in quatrefoil suspension gyroscopes including mode alignment and frequency tuning. The mode alignment voltage control precisely aligns the modes to the electrodes used to drive, sense and tune the modes thereby facilitating independent control of both modes. Subsequently, a tuning voltage is applied to increase the effective stiffness of the first mode by decreasing the potential difference between the ring and the electrodes aligned with the antinodes of the first mode. This approach to mode-matching is successfully implemented in multiple device prototypes. There is a significant improvement in the mechanical sensitivity by implementing mode-matching as predicted by modeling. The measured scale factor improvement matches closely with the estimated mechanical scale factor over the entire tuning range. The tuning voltage required as predicted by a theoretical model matches closely with the results of the measurements. Future work will focus on the implementation of automatic mode matching for gyroscope operation.

References

[1] I. P. Prikhodko, J. A. Gregory, W. A. Clark, J. A. Geen, M. W. Judy, C. H. Ahn, and T. W. Kenny. Mode-matched mems coriolis vibratory gyroscopes: Myth or reality? In *2016 IEEE/ION Position, Location and Navigation Symposium (PLANS)*, pages 1–4, 2016.

[2] S. A. Zotov, A. A. Trusov, and A. M. Shkel. High-range angular rate sensor based on mechanical frequency modulation. *Journal of Microelectromechanical Systems*, 21(2):398–405, 2012.

[3] X. Wei and A. A. Seshia. Analytical formulation of modal frequency split in the elliptical mode of scs micromechanical disk resonators. *Journal of Micromechanics and Microengineering*, 24(2):025011, 2014.

[4] M. Parajuli, G. Sobreviela, and A. A. Seshia. Electrostatic frequency tuning of bulk acoustic wave disk gyroscopes. In *2020 Joint Conference of the IEEE International Frequency Control Symposium and International Symposium on Applications of Ferroelectrics (IFCS-ISAF)*, pages 1–4, 2020.

[5] D. Kim and R. M'Closkey. A mem vibratory gyro with mode-matching achieved by resonator mass loading. In *2014 IEEE/ION Position, Location and Navigation Symposium - PLANS 2014*, pages 499–503, 2014.

[6] Z. Liu, A. Daruwalla, B. Hamelin, and F. Ayazi. A study of mode-matching and alignment in piezoelectric disk resonator gyros via femtosecond laser ablation. In *2021 IEEE 34th International Conference on Micro Electro Mechanical Systems (MEMS)*, pages 342–345, 2021.

[7] A. Mustafazade, M. Pandit, C. Zhao, G. Sobreviela, Z. Du, P. Steinmann, X. Zou, R. T. Howe, and A. A. Seshia. A vibrating beam mems accelerometer for gravity and seismic measurements. *Scientific reports*, 10(1):1–8, 2020.

[8] M. Parajuli, G. Sobreviela, and A. A. Seshia. Silicon mems gyroscope with quatrefoil suspension system achieving 1 million quality factor. In *2022 IEEE 35th International Conference on Micro Electro Mechanical Systems Conference (MEMS)*, pages 770–773, 2022.